Note added in proof: Another group has recently determined the structure of the bovine poly(A) polymerase (*28*).

References and Notes

1. Y. Huang and G. C. Carmichael, *Mol. Cell. Biol.* **16**, 1534 (1996).
2. A. J. Carpousis, N. F. Vanzo, L. C. Raynal, *Trends Genet.* **15**, 24 (1999).
3. A. B. Sachs, P. Sarnow, M. W. Hentze, *Cell* **89**, 831 (1997).
4. G. A. Coburn and G. A. Mackie, *Prog. Nucleic Acid Res. Mol. Biol.* **62**, 55 (1999).
5. J. Zhao, L. Hyman, C. Moore, *Microbiol. Mol. Biol. Rev.* **63**, 405 (1999).
6. M. Ohnacker, L. Minvielle-Sebastia, W. Keller, *Nucleic Acids Res.* **24**, 2585 (1996).
7. G. Martin and W. Keller, *EMBO J.* **15**, 2593 (1996).
8. L. Holm and C. Sander, *Trends Biochem. Sci.* **20**, 345 (1995).
9. Untagged PAP was expressed and purified essentially as described (*10*), with the exception that the published heparin purification step was replaced with a Source S (Pharmacia) chromatography step. The peak fractions were concentrated to 40 mg/ml using a finger dialysis concentrator (Schleicher & Shuell, Keene, NH), exchanged into 75 mM NaCl, 10 mM sodium phosphate (pH 6.8), 2 mM $MgCl_2$, 1 mM dithiothreitol (DTT), and 20% glycerol and stored at −80°C, prior to crystallization. Typical yields of pure protein from this procedure were 1.2 mg/liter of *E. coli* culture for the full-length PAP, and 2.2 mg/liter culture for the Δ10 truncation. Selenomethionine was incorporated into the protein using an auxotrophic strain of *E. coli* into which the pLysS plasmid had been transformed and M9 growth media in which selenomethionine replaced methionine. The purification of the selenomethionine-incorporated protein was identical to that described above, however, the yield was significantly lower. PAP was crystallized at 4°C by vapor diffusion in hanging drops over wells containing 13.5% ethylene glycol, 9% PEG 8K, 6% glycerol, 100 mM Hepes (pH 7.24), and 2 mM DTT. The crystallization drops contained equal volumes of well solution and concentrated protein. Although full-length, bacterially-produced Pap1 is soluble to at least 35 mg/ml, it does not form crystals, and from dynamic light scattering measurements, it appears to be significantly aggregated. Crystals of Pap1 were initially grown using a 25–amino acid COOH-terminal deletion of the full length protein generated with endoproteinase Glu-C. The endoproteases Lys-C, thermolysin, and chymotrypsin produced similar fragments, suggesting that the COOH-terminus of Pap1 is intrinsically flexible. To improve the reproducibility of crystallization and quality of diffraction, data was collected from crystals formed from a previously characterized truncation of Pap1, Δ10PAP.
10. A. M. Zhelkovsky, M. M. Kessler, C. L. Moore, *J. Biol. Chem.* **270**, 26715 (1995).
11. MAD data (ALS, Berkeley, CA) was processed with MOSFLM and SCALA (*29*). Data from the Advanced Photon Source (Argonne, IL) beamline 19-ID was processed with HKL2000. Rotating anode data was processed with XDS (*30*). Eight of the 16 selenium positions were found by SOLVE (*31*), and the remaining sites were found by difference Fourier methods using solvent flattened phases derived from the initial selenium sites. Phase refinement was initially done using G. Van Duyne's GVX suite. Later, SHARP (*32*) was used to improve the quality of the selenomethionine MAD maps. The model was built using O (*33*) and refined using the simulated annealing torsion angle refinement protocol in CNS (*34*).
12. D. L. Ollis, P. Brick, R. Hamlin, N. G. Xuong, T. A. Steitz, *Nature* **313**, 762 (1985).
13. C. A. Brautigam and T. A. Steitz, *Curr. Opin. Struct. Biol.* **8**, 54 (1998).
14. A. Zhelkovsky, S. Helmling, C. Moore, *Mol. Cell. Biol.* **18**, 5942 (1998).
15. H. Pelletier, M. R. Sawaya, A. Kumar, S. H. Wilson, J. Kraut, *Science* **264**, 1891 (1994).
16. L. C. Pedersen, M. M. Benning, H. M. Holden, *Biochemistry* **34**, 13305 (1995).
17. Although PAPs are more active and less selective in the presence of Mn^{2+}, no significant differences between the $MgCl_2$- and $MnCl_2$-soaked crystals were seen at this resolution. The structure presented here has been refined against the $MnCl_2$ data because these data were of better quality. The identity of the manganese sites was confirmed by examining anomalous difference Fourier maps.
18. Initial difference Fourier maps were unclear about the orientation of the base. Refinement using a beta-version of BUSTER (*35*) showed the orientation of the base clearly. Subsequent refinement in CNS allowed unambiguous observation of the base in CNS simulated annealing omit maps.
19. S. Doublie, M. R. Sawaya, T. Ellenberger, *Struct. Folding Des.* **7**, R31 (1999).
20. The functional group of N226 is 4.4 Å away from N6 in the more closed copy of the complex, and 5.1 Å away from N6 in the more open copy of the complex.
21. Mutation of V141 to phenylalanine reduces the catalytic activity of Pap1 by more than 90% and causes a sixfold increases in the K_m for primer (A. M. Zhelkovsky, S. Helmling, C. L. Moore, unpublished data).
22. We believe that the pyrophosphate seen in the 3′-dATP soak was produced by a spurious reaction in which 3′-dATP was hydrolyzed to 3′-dAMP and inorganic pyrophosphate (PP_i). Data collected from crystals soaked in α-β-CH_2-ATP, a nonhydrolyzable ATP analog, do not show the pyrophosphate density.
23. L. S. Beese, J. M. Friedman, T. A. Steitz, *Biochemistry* **32**, 14095 (1993).
24. S. Doublie and T. Ellenberger, *Curr. Opin. Struct. Biol.* **8**, 704 (1998).
25. The proteolytic susceptibility of the C-RBS by endoproteinase Lys-C (A. Bohm, unpublished results) supports the notion that this region of the molecule may be intrinsically disordered.
26. S. C. Agalarov, G. Sridhar Prasad, P. M. Funke, C. D. Stout, J. R. Williamson, *Science* **288**, 107 (2000).
27. M. R. Conte *et al.*, *EMBO J.* **19**, 3132 (2000).
28. G. Martin, W. Keller, S. Doublie, *EMBO J.*, in press.
29. Collaborative Computational Project, *Acta Crystallogr. D* **50**, 760 (1994).
30. W. Kabsch, *J. Appl. Crystallogr.* **26**, 795 (1993).
31. T. C. Terwilliger and J. Berendzen, *Acta Crystallogr. D* **55**, 849 (1999).
32. E. de La Fortelle and G. Bricogne, *Methods Enzymol.* **276**, 472 (1997).
33. T. A. Jones, J. Y. Zou, S. W. Cowan, M. O. Kjeldgaard, *Acta Crystallogr. A* **47**, 110 (1991).
34. A. T. Brünger *et al.*, *Acta Crystallogr. D* **54**, 905 (1998).
35. G. Bricogne, *Methods Enzymol.* **276**, 361 (1997).
36. S. Doublie, S. Tabor, A. M. Long, C. C. Richardson, T. Ellenberger, *Nature* **391**, 251 (1998).
37. P. J. Kraulis, *J. Appl. Crystallogr.* **24**, 946 (1991).
38. BOBSCRIPT, version 2.4; R. Esnouf, Oxford University.
39. M. R. Sawaya, R. Prasad, S. H. Wilson, J. Kraut, H. Pelletier, *Biochemistry* **36**, 11205 (1997).
40. A. Nicholls, J. Bharadwaj, B. Honig, *Biophys. J.* **64**, 166 (1993).

41. We thank W. Somers for the use of computing facilities to run BUSTER and N. Duke, V. Srajer, and C. Ogata for their help collecting data. Also, we thank D. Jeruzalmi for his program R3D_TO_POV and for his help in interpreting the structure. This work was supported by NIH grant R01 GM57218-01A2 and American Cancer Society grant RPG-99-104-01-TBE. Coordinates for the complexed structure have been submitted to Protein Data Base (1FA0).

9 June 2000; accepted 13 July 2000

Differential Clustering of CD4 and CD3ζ During T Cell Recognition

Matthew F. Krummel,[1] Michael D. Sjaastad,[2] Christoph Wülfing,[1]* Mark M. Davis[1]†

Whereas T helper cells recognize peptide–major histocompatibility complex (MHC) class II complexes through their T cell receptors (TCRs), CD4 binds to an antigen-independent region of the MHC. Using green fluorescent protein–tagged chimeras and three-dimensional video microscopy, we show that CD4 and TCR-associated CD3ζ cluster in the interface coincident with increases in intracellular calcium. Signaling-, costimulation-, and cytoskeleton-dependent processes then stabilize CD3ζ in a single cluster at the center of the interface, while CD4 moves to the periphery. Thus, the CD4 coreceptor may serve primarily to "boost" recognition of ligand by the TCR and may not be required once activation has been initiated.

In higher vertebrates, T lymphocytes systematically scan cells and tissues for non-self antigens embedded in molecules of the MHC. Recognition of these peptide-MHC complexes is achieved through the αβ TCR, and signal transduction occurs through phosphorylation of the tightly associated CD3 γ, δ, ε, and ζ polypeptides (*1*). Several receptors on T cells can potentiate the response of the T cell, and their engagement is often required for successful activation in vivo. One of these is CD4 on T helper cells, which binds to relatively invariant sites on MHC class II molecules outside the peptide-binding groove (*2*, *3*) and accumulates at the T cell–antigen-presenting cell (APC) interface (*4*). During activation, CD4 increases T

[1]Department of Microbiology and Immunology, Stanford University School of Medicine, and the Howard Hughes Medical Institute, Stanford, CA 94305, USA. [2]Universal Imaging Corporation, 502 Brandywine Parkway, West Chester, PA 19380, USA.

*Present address: Center for Immunology, University of Texas Southwestern Medical Center, 5323 Harry Hines Boulevard, Dallas, TX 75390–9093, USA.

†To whom correspondence should be addressed: E-mail: mdavis@cmgm.stanford.edu

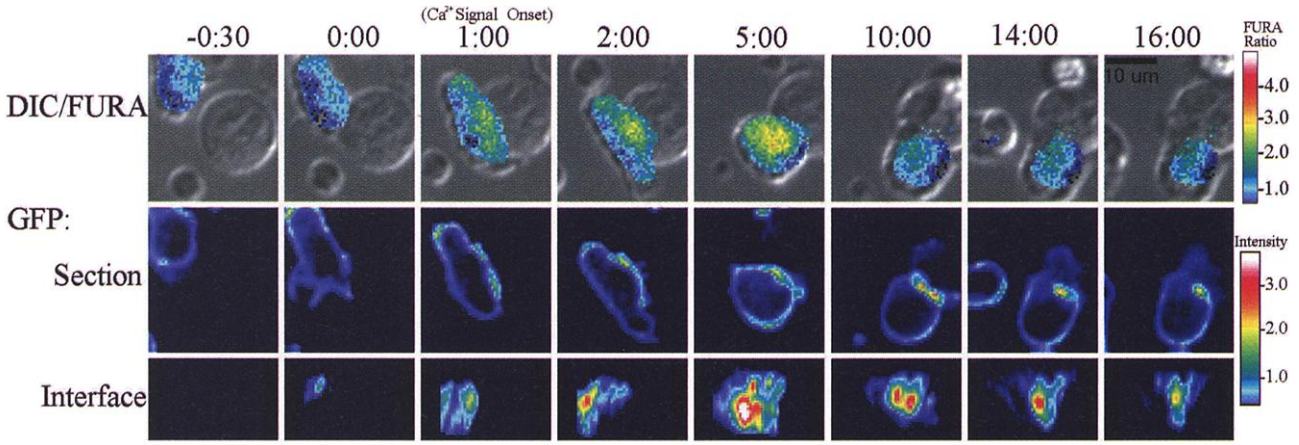

Fig. 1. Clustering of CD3ζ during the onset of signaling, followed by mature synapse formation. CD3ζ-GFP T cells and strong agonist (10 μM)–pulsed CH27 cells were mixed on coverslips and imaged at 15-s intervals. Each time point shows the DIC image overlayed with the calcium ratio obtained with FURA-2 (340/380), a mid-cell *z* section of GFP, and projection of the contact-region view obtained by a Max Intensity method. The Max Intensity projection method was applied to a region encompassing the interface [assessed by the DIC image (*20*)]. Times relative to the onset of the calcium signal are indicated. Pixel values within the resulting central-core clusters were typically at least twice the intensity of the average pixel located along the cell surface. Concentrations of CD3ζ-GFP at the trailing edge, opposite the site where the interface most often forms, are often observed before the first calcium flux, and these typically shifted forward in the first minutes after activation. Within minutes of forming, these larger clusters often diminish in intensity, probably as a result of receptor internalization (*33*). Occasionally, a small region of internalized GFP was briefly (≤30 s) observed just under the interface, suggesting that internalized receptors and/or GFP are quickly proteolysed or inactivated. We have observed these same phenomena with tagged CD3δ and TCRα constructs (*34*). Time-lapse movies of these and other CD3ζ-GFP accumulations are available in Web fig. 2 (*17*).

cell sensitivity to antigen by 10- to 100-fold (*5*–*7*). A cysteine motif present in the CD4 tail binds src-family kinase $p56^{lck}$ (*8*), and Lck appears to be responsible for phosphorylating CD3ζ, the earliest known event in T cell signaling (*9*).

Despite CD4's importance in generating signals, its role in potentiating TCR recognition remains unclear. TCR binding affinity varies considerably (*10*), and it has been suggested that CD4 binds MHC class II simultaneously with the TCR (*11*) or perhaps shortly after TCR–peptide-MHC engagement (*6*, *7*) and serves to stabilize the complex. Recently it has been shown that some of the signaling molecules involved in T cell recognition do not form a homogeneous "cap" but rather segregate into distinct areas of the T cell–APC interface, forming a "supramolecular activation cluster" (SMAC) (*12*) and contributing to what has been called the "immunological synapse" (*13*). By antibody staining of fixed cells (*12*), or by individually labeling molecules in a lipid bilayer in place of the APC (*13*), it has been shown that after just a few minutes of T cell coupling, TCRs on T cells and MHC molecules on APCs segregate to the central core of the contact zone surrounded by lymphocyte function–associated antigen-1 (LFA-1) and intracellular adhesion molecule–1 (ICAM-1) accumulations, respectively.

In order to analyze the role of CD4 and CD3ζ during synapse formation, we made COOH-terminal fusions of these molecules with green fluorescent protein (GFP) as described for ICAM-1 (*14*) and separately transfected them into the T cell line D10 (*15*, *16*). The clones analyzed had moderate levels of surface GFP expression and were indistinguishable from the parental line in their responses to antigens (Web fig. 1A) (*17*). Additionally, CD3ζ-GFP and CD4-GFP associate with ZAP-70 and Lck, respectively, and CD3ζ-GFP was phosphorylated in response to signaling (Web fig. 1B) (*17*). The cells were analyzed with an instrument that coordinated a high-speed piezoelectric objective positioning device to rapidly change the focal plane while "streaming" the acquired data from a fast-cooled charge-coupled device camera. Twenty optical sections through a T cell–APC couple were captured within a 3-s window, and calcium and bright-field images were collected within an additional 2 s.

In Fig. 1, the response of D10 CD3ζ-GFP cells to peptide-loaded CH27 (*18*) after correcting for photobleaching and background (*19*) shows CD3ζ clustering in the contact area coincident with the rise in intracellular calcium. Such clusters were typically very dynamic, forming, breaking apart, and reforming over time, but ultimately coalesced into a single, large central cluster.

CD4-GFP accumulation was initially very similar to that of CD3ζ, with punctate accumulations forming coincident with calcium mobilization (Fig. 2). However, starting at about 2 min after calcium signaling, CD4-GFP was frequently diminished in the central interface. This appears as a ring when the interface is viewed en face, and similar structures were observed within 15 min of activation in 69% ($n = 29$) of T cells responding to 10 μM CA 134-147. Both wide exclusions (reaching the perimeter of the contact zone) and very narrow exclusions (~2 μM in diameter) were observed and in most cases decreased in diameter over time. The distinct pattern of CD3ζ versus CD4 localization seen with GFP fusions was also confirmed by antibody staining of fixed T-B cell conjugates (Web fig. 4) (*17*).

The appearance of stable CD3ζ and CD4 accumulations was highly coincident with the onset of calcium signaling, and the magnitude of the maximum intensity (*20*) correlated with the concentration of antigenic peptide (Web fig. 5A) (*17*). When challenged with weak agonists or with no peptide at all, T cells interfaces typically did not show appreciable, stable accumulation of CD3ζ-GFP or CD4-GFP and frequently had an excluded appearance (Web fig. 5B) (*17*). Strong-agonist–mediated clusters slowly decrease in number over time as they coalesce into the center of the interface, while the brightest cluster increases in intensity, indicating that small clusters are merging into larger ones (Fig. 3). Weak-agonist peptide stimulation gave clusters that generally lasted only one frame or less (~15 s).

The formation of a stable synapse was modulated by peptide concentration and was severely compromised by blocking either the calcium increase ($BAPTA/Ni^{2+}$) or cytoskeletal rearrangement (Cytochalasin D or LAT-A), although neither prevented the formation of transient CD3ζ clusters (Web table 1). Blocking B7 costimulation allowed transient clustering and calcium increase, but the frequency of stable CD3ζ accumulations was reduced by about fivefold. Similar cytoskeletal and costimulation dependence is observed for the clustering of labeled MHC molecules on APCs during T cell

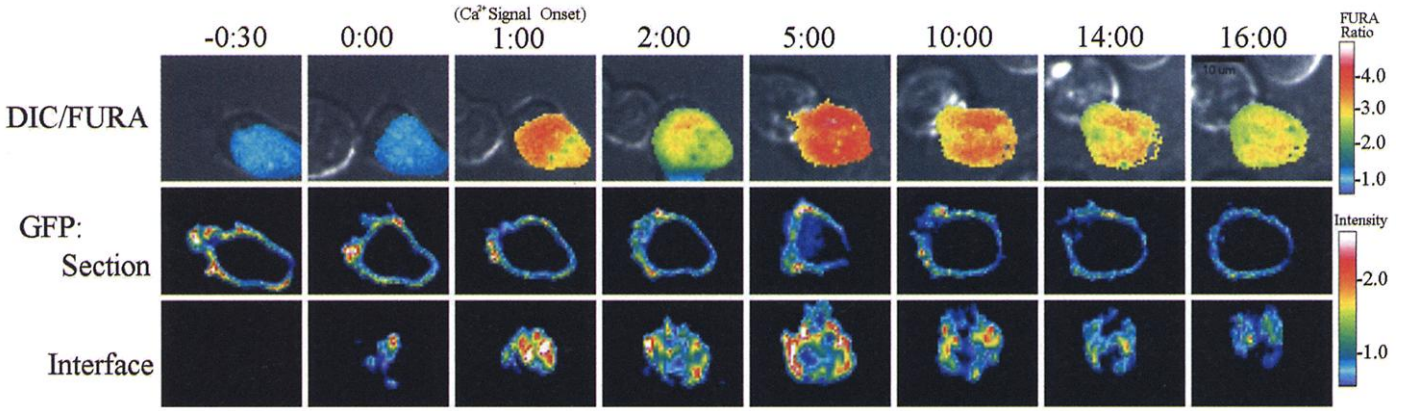

Fig. 2. Clustering of CD4 during the onset of signaling followed by mature synapse formation. Clustering patterns of CD4-GFP indicate an early recruitment and subsequent exclusion at the T cell–APC interface. D10 CD4-GFP clones were imaged while interacting with strong agonist (10 μM)–pulsed CH27 cells. Typical accumulations in the interface were only twofold higher than average cell membrane intensities. CD4 exclusions occasionally collapsed and re-formed during the minutes after activation. This pattern was also evident at similar frequencies when lower peptide concentrations were used, and where no clear exclusion was observed, CD4-GFP accumulations appeared as actively moving patches. A time-lapse movie of this and other CD4-GFP accumulations is available in Web fig. 3 (*17*).

recognition (*21*). Previous work has shown that costimulation triggers a cytoskeleton-dependent movement of membrane patches (rafts) (*22*, *23*) into the interface, and it seems likely that this helps to create and maintain the central accumulation, particularly because CD3ζ associates with the cytoskeleton in activated T cells (*24*, *25*).

To examine the coordination of these molecules, we first treated T cells with antibody Fab fragments before adding APCs. Treatment with antibody to CD4 (anti-CD4) prevented CD4-GFP accumulation, slightly reduced CD3ζ GFP accumulation, and significantly inhibited calcium mobilization (Web fig. 6) (*17*). Anti-TCR blockade prevented CD3ζ-GFP accumulation and calcium increase and abolished the high-density accumulation of CD4-GFP. Thus, CD4 accumulation is dependent on TCR binding and/or signaling even though its ligand (MHC class II) is present on B cells, suggesting that some feature of early TCR–peptide-MHC recognition serves to recruit CD4 to the interface and initiate signaling. This is not a function of the cytoplasmic tail because a deletion mutant behaved in the same way as the intact molecule (Web fig. 7) (*17*).

In this work we have shown two phenomena relevant to T cell recognition: (i) the appearance of small, dispersed clusters of CD3ζ and CD4 that appear at the same time as the initial calcium response and that, if a sufficient amount of agonist peptide is present, adopt a mature synapse structure and (ii) the differential accumulation of CD3ζ versus CD4.

The initiation of activation in the T cell did not correlate with the formation of the SMAC/synapse structure described by Monks *et al.* (*12*) and Grakoui *et al.* (*13*), but rather with the formation of much smaller, very unstable clusters of CD3ζ and CD4.

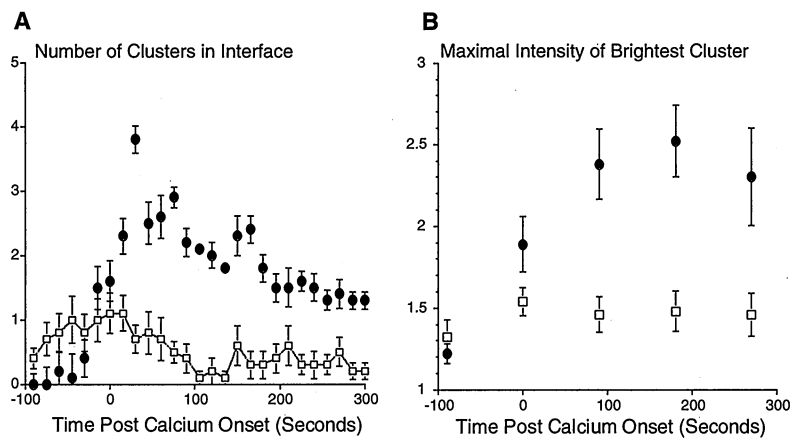

Fig. 3. Coalescence of multiple clusters into a central core cluster. (**A**) The number of discrete clusters within the interface at various times after the calcium signal onset mediated by APC pulsed with strong agonist (CA 134-147) (●) or weak agonist (E8T) (□) at 10 μM. At 15-s intervals relative to the calcium signaling onset (FURA ratio >150% of nonreacting level), the number of individual clusters, defined as contiguous regions within the interface with GFP intensities of >100% above the cell surface average, were counted. Data show the mean ± SEM for 15 couples. (**B**) The brightest single-pixel intensity at the front of the cell was compared to the average cell-surface pixel intensity to obtain a ratio. This corresponds to the degree of aggregation of the brightest cluster in the contact zone. Data show the mean ± SEM from scoring 15 couples for each condition in which a calcium ratio change was observed. This allows a consistent and activation-relevant reference point to be used, and those E8T-mediated couples that did not induce calcium signals were similarly unable to mediate stable clustering or coalescence of clusters.

These clusters were also seen with weak agonists, although in those situations they rarely coalesced into large, central groupings. Such clusters may represent the initiators of activation, or perhaps even smaller TCR aggregates are the primary initiators (*26*, *27*).

In the case of histamine receptor signaling, threshold levels of calcium can be reached by a combination of frequency, amplitude, and the integration of signals from multiple dispersed receptor clusters (*28*). We suggest that a similar process occurs with T cell signaling and is responsible for the initiation of T cell activation. This early "fluid" phase might be driven by specific TCR-p/MHC oligomerization, as observed in solution studies (*29*) and independent of the cytoskeleton. Soon after signaling is initiated, however, CD3ζ and other molecules would move into the center of the interface by costimulation-induced, cytoskeleton-mediated membrane raft movement (*22*, *23*). This stable accumulation is likely to be required for sustained signaling and subsequent progression to full activation and cytokine secretion (*30*).

With respect to the differential localization of CD4 versus CD3ζ, these findings do not support a model in which CD4 acts to stabilize the TCR-pMHC complexes. No ev-

idence for such stabilization has been seen in solution studies, and direct MHC class II–CD4 binding was not detected (*31*). These results and the data presented here instead suggest that the function of CD4 may be to "boost" or "trigger" the early phase of activation. Once that process is under way, CD4 seems to be excluded from the central core of the synapse, perhaps owing to the formation of some lattice-like structure by the remaining molecules.

References and Notes

1. A. Weiss and D. R. Littman, *Cell* **76**, 263 (1994).
2. R. König, L. Huang, R. N. Germain, *Nature* **356**, 796 (1992).
3. G. Cammarota *et al.*, *Nature* **356**, 799 (1992).
4. A. Kupfer and S. J. Singer, *J. Exp. Med.* **170**, 1697 (1989).
5. P. Marrack *et al.*, *J. Exp. Med.* **158**, 1077 (1983).
6. J. Hampl, Y-H. Chein, M. M. Davis, *Immunity* **7**, 379 (1997).
7. J. Madrenas, L. A. Chau, J. Smith, J. A. Bluestone, R. N. Germain, *J. Exp. Med.* **185**, 219 (1997).
8. J. M. Turner *et al.*, *Cell* **60**, 755 (1990).
9. D. B. Straus and A. Weiss, *Cell* **70**, 585 (1992).
10. M. M. Davis *et al.*, *Annu. Rev. Immunol.* **16**, 523 (1998).
11. C. A. Janeway Jr., *Annu. Rev. Immunol.* **10**, 645 (1992).
12. C. R. F. Monks, B. A. Freiberg, H. Kupfer, N. Sciaky, A. Kupfer, *Nature* **395**, 82 (1998).
13. A. Grakoui *et al.*, *Science* **285**, 221 (1999).
14. C. Wülfing, M. D. Sjaastad, M. M. Davis, *Proc. Natl. Acad. Sci. U.S.A.* **95**, 6302 (1998).
15. J. Kaye, S. Porcelli, J. Tite, B. Jones, C. A. Janeway Jr., *J. Exp. Med.* **158**, 836 (1983).
16. GFP fusion constructs were transfected into D10 by electroporation as described (*32*). After 1 to 2 weeks, these cultures were expanded into 24-well dishes, screened by flow cytometry, and sorted for GFP expression. Established clones were subjected to phenotypic analysis by staining for CD4, CD3ε, TCR, CD28, and CD25 as well as proliferation analysis against CA 134-147 and the variant peptides E8T and I5G.
17. Supplemental Web material is available at *Science* Online at www.sciencemag.org/feature/data/1050535.shl.
18. Clones were maintained by weekly restimulations as described (*15*), except that cultures were typically not supplemented with exogenous interleukin-2. Activation experiments were performed from 5 to 10 days after the stimulation culture. CH27 is a B cell lymphoma that expresses IA^k, B7-1, and B7-2. Experiments were done at 37°C as described (*14*).
19. GFP intensity data were corrected both for background intensity and for photobleaching. Background level was measured by imaging a dish in the absence of cells. This background level was subtracted from intensity data to obtain background-subtracted data sets. For bleaching, a nonreactive cell was analyzed for surface intensity over time, and the intensity over time was fitted to an exponential decay curve ($I_t = I_0 10^{kt}$, where k is the decay constant, t is the number of times the fluorophore was illuminated at a constant rate, and I_t and I_0 are the initial intensities and intensities at time t). The decay constant k was used to calculate a correction factor ($1/10^{kt}$) for each time point in the experimental data sets. Typical decay constants were ~0.01, giving half-lives of about 30 illuminations. Typical experiments involved about 60 to 80 illuminations.
20. Intensities from 340- and 380-nm excitations of Fura-2 were used to make a ratio image. Background calcium levels were obtained from at least five frames before activation and were similar to nonreactive cells from other portions of the field. Increases of 30% above background were found to be well above random fluctuations, and the onset of agonist-driven reactions typically was characterized by at least a 100% increase in a single 15-s time period. Individual cells were analyzed for maximal pixel intensities along the leading edge of cells by a line-scan function. All collected z planes were analyzed and compared to the average from three intensity line scans (taken at different z planes) around the circumference of the cell of interest. Background- and bleach-corrected data were used for all analyses. Rectangular x-y regions encompassing the estimated interface were determined from the differential interference contrast (DIC) image, and z stacks encompassing these regions were used for the interface projections. Max Intensity Projections were used (Metamorph, Universal Imaging, PA).
21. C. Wülfing and M. M. Davis, unpublished observations.
22. ———, *Science* **282**, 2266 (1998).
23. A. Viola, S. Schroeder, Y. Sakakibara, A. Lanzavecchia, *Science* **283**, 680 (1999).
24. S. Caplan, S. Zeliger, L. Wang, M. Baniyash, *Proc. Natl. Acad. Sci. U.S.A.* **92**, 4768 (1995).
25. M. M. Rozdzial, B. Malissen, T. H. Finkel, *Immunity* **3**, 623 (1995).
26. J. R. Cochran, T. O. Cameron, L. J. Stern, *Immunity* **12**, 241 (2000).
27. J. J. Boniface *et al.*, *Immunity* **9**, 459 (1998).
28. M. D. Bootman, M. J. Berridge, P. Lipp, *Cell* **91**, 367 (1998).
29. Z. Reich *et al.*, *Nature* **387**, 617 (1997).
30. P. A. Negulescu, N. Shastri, M. D. Calahan, *Proc. Natl. Acad. Sci. U.S.A.* **91**, 2873 (1994).
31. N. Barclay and P. A. van der Merwe, unpublished observations.
32. J. Kaye and S. M. Hedrick, *Nature* **336**, 580 (1988).
33. A. Viola and A. Lanzavecchia, *Science* **273**, 104 (1996).
34. M. F. Krummel, M. D. Sjaastad, C. Wülfing, M. M. Davis, data not shown.

35. We are grateful to J. Huppa, C. Sumen, and L. Richie for critical comments and advice. We thank C. Terhorst and J. Parnes for supplying the cDNAs for CD3ζ and CD4, respectively. We also thank the Stanford Shared FACS Facility for assistance in cell sorting. Supported by a postdoctoral award from the National Institutes of Health (M.F.K.) and by the Howard Hughes Medical Institute and NIH.

20 March 2000; accepted 13 July 2000

Treatment of Murine Colitis by *Lactococcus lactis* Secreting Interleukin-10

Lothar Steidler,[1]*† Wolfgang Hans,[1]† Lieven Schotte,[1] Sabine Neirynck,[1] Florian Obermeier,[2] Werner Falk,[2] Walter Fiers,[1] Erik Remaut[1]

The cytokine interleukin-10 (IL-10) has shown promise in clinical trials for treatment of inflammatory bowel disease (IBD). Using two mouse models, we show that the therapeutic dose of IL-10 can be reduced by localized delivery of a bacterium genetically engineered to secrete the cytokine. Intragastric administration of IL-10–secreting *Lactococcus lactis* caused a 50% reduction in colitis in mice treated with dextran sulfate sodium and prevented the onset of colitis in IL-$10^{-/-}$ mice. This approach may lead to better methods for cost-effective and long-term management of IBD in humans.

Inflammatory bowel disease (IBD), including Crohn's disease and ulcerative colitis, is a significant public health problem in Western societies, affecting 1 in 1000 individuals, yet its etiology remains poorly understood. IBD is characterized clinically by chronic inflammation in the large and/or small intestine, the symptoms of which include diarrhea, abdominal pain, weight loss, and nausea. Death can result, in extreme cases, from malnutrition, dehydration, and anemia. IBD is thought to arise from interacting genetic and environmental factors (*1*) and may involve abnormal T cell responses to commensal microflora (*2–4*). Biologically based therapies such as antibodies to tumor necrosis factor (TNF), which is a strong proinflammatory mediator (*5–7*), and recombinant IL-10 (*8*) can ameliorate the disorder.

Because IL-10 has a central role in downregulating inflammatory cascades (*9*) and matrix metalloproteinases (*10*), it is a likely candidate for use in therapeutic intervention. In this study we have tested a new method of delivering IL-10: in situ synthesis by genetically engineered bacteria (*Lactococcus lactis*), in two mouse models of the disease, one involving treatment of chronic colitis induced by 5% dextran sulfate sodium (DSS) (*11*) and one involving prevention of colitis that spontaneously develops in IL-$10^{-/-}$ mice (*12*). We show that this approach, which depends on in vivo synthesis of IL-10, requires much lower doses than systemic treatment. Neither mouse model mimics all aspects of human IBD, but such models are essential for development of new therapeutic approaches to IBD (*13–20*).

L. lactis is a nonpathogenic, noninvasive, noncolonizing Gram-positive bacterium, mainly used to produce fermented foods. We previously constructed recombinant *L. lactis* strains for production and in vivo delivery of cytokines

[1]Department of Molecular Biology, Ghent University and Flanders Interuniversity Institute for Biotechnology, K. L. Ledeganckstraat 35, 9000 Gent, Belgium. [2]Department of Internal Medicine I, University of Regensburg, Franz-Josef-Strauss-Allee 11, 93042 Regensburg, Germany.

*To whom correspondence should be addressed. E-mail: lothar.steidler@dmb.rug.ac.be

†These authors contributed equally to this work.